Research Article

Nano Research
2020, 13(12): 3358–3363

ISSN 1998-0124 CN 11-5974/O4
https://doi.org/10.1007/s12274-020-3021-4

Room temperature ferromagnetism in ultra-thin van der Waals crystals of 1T-$CrTe_2$

Xingdan Sun[1,2,§], Wanying Li[1,2,§], Xiao Wang[3,4,5,§], Qi Sui[6,§], Tongyao Zhang[7,8], Zhi Wang[1,2], Long Liu[1,2], Da Li[1,2], Shun Feng[1,2,11], Siyu Zhong[9], Hanwen Wang[1,2], Vincent Bouchiat[10], Manuel Nunez Regueiro[10], Nicolas Rougemaille[10], Johann Coraux[10], Anike Purbawati[10], Abdellali Hadj-Azzem[10], Zhenhua Wang[1,2], Baojuan Dong[7,8], Xing Wu[9], Teng Yang[1,2] (✉), Guoqiang Yu[3,4,5] (✉), Bingwu Wang[6] (✉), Zheng Han[1,2,7] (✉), Xiufeng Han[3,4,5], and Zhidong Zhang[1,2]

[1] *Shenyang National Laboratory for Materials Science, Institute of Metal Research, Chinese Academy of Sciences, Shenyang 110016, China*
[2] *School of Material Science and Engineering, University of Science and Technology of China, Hefei 230026, China*
[3] *Beijing National Laboratory for Condensed Matter Physics, Institute of Physics, Chinese Academy of Sciences, Beijing 100190, China*
[4] *Center of Materials Science and Optoelectronics Engineering, University of Chinese Academy of Sciences, Beijing 100049, China*
[5] *Songshan Lake Materials Laboratory, Dongguan 523808, China*
[6] *Beijing National Laboratory for Molecular Sciences, Beijing Key Laboratory of Magnetoelectric Materials and Devices, College of Chemistry and Molecular Engineering, Peking University, Beijing 100871, China*
[7] *Collaborative Innovation Center of Extreme Optics, Shanxi University, Taiyuan 030006, China*
[8] *State Key Laboratory of Quantum Optics and Quantum Optics Devices, Institute of Opto-Electronics, Shanxi University, Taiyuan 030006, China*
[9] *Shanghai Key Laboratory of Multidimensional Information Processing Department of Electrical Engineering, East China Normal University, 500 Dongchuan Road, Shanghai 200241, China*
[10] *University Grenoble Alpes, CNRS, Grenoble INP, Institut Néel, F-38000 Grenoble, France*
[11] *School of Physical Science and Technology, ShanghaiTech University, Shanghai 200031, China*
[§] *Xingdan Sun, Wanying Li, Xiao Wang, and Qi Sui contributed equally to this work.*

Received: 8 June 2020 / **Revised:** 4 July 2020 / **Accepted:** 29 July 2020

ABSTRACT

Although many emerging new phenomena have been unraveled in two dimensional (2D) materials with long-range spin orderings, the usually low critical temperature in van der Waals (vdW) magnetic material has thus far hindered the related practical applications. Here, we show that ferromagnetism can hold above 300 K in a metallic phase of 1T-$CrTe_2$ down to the ultra-thin limit. It thus makes $CrTe_2$ so far the only known exfoliated ultra-thin vdW magnets with intrinsic long-range magnetic ordering above room temperature. An in-plane room-temperature negative anisotropic magnetoresistance (AMR) was obtained in ultra-thin $CrTe_2$ devices, with a sign change in the AMR at lower temperature, with −0.6% and +5% at 300 and 10 K, respectively. Our findings provide insights into magnetism in ultra-thin $CrTe_2$, expanding the vdW crystals toolbox for future room-temperature spintronic applications.

KEYWORDS

room temperature ferromagnetism, two dimensional (2D), $CrTe_2$, anisotropic magnetoresistance (AMR)

1 Introduction

Two-dimensional (2D) van der Waals (vdW) ferromagnetic layers have been a cutting-edge topic in recent years, as they not only provide opportunities for new-concept nanostructures [1–5], but also serve as a test-bed for novel spin physics [6, 7]. Especially, spintronic devices built with vdW magnets have aroused great interest [8]. For example, magnetoresistance in spin-filtered magnetic vdW heterojunctions was manifested to be as high as 19,000%, far superior to that of conventionally grown magnetic thin films [9]. More recently, a current-induced magnetic switch was demonstrated with few layers of Fe_3GeTe_2 [10], suggesting that such materials are valuable ingredients for nanoelectronics. However, most of the reported vdW spintronic devices are functioning at low temperature, which are practically not preferable. Interestingly, even in some of those vdW magnets with relatively low intrinsic Curie temperature (T_C) such as Fe_3GeTe_2, room temperature 2D ferromagnetism may be realized via certain extrinsic manners, such as strong electron doping with an ionic gate [5], or an enhancement of magnetic anisotropy energy through a micrometer-sized geometric confinement [11]. Nevertheless, these methods are in principle incompatible with larger scale solid-state device applications. Demonstrations of spintronic devices based on intrinsic room-temperature ferromagnetic vdW materials remain challenging.

Address correspondence to Teng Yang, yangteng@imr.ac.cn; Bingwu Wang, wangbw@pku.edu.cn; Guoqiang Yu, guoqiangyu@iphy.ac.cn; Zheng Han, vitto.han@gmail.com

To date, while there are theoretical predictions [12–14], intrinsic vdW ferromagnets with T_C above 300 K have been experimentally reported in a very limited library of materials, including epitaxially or chemical vapour/exfoliation synthesized 2D films of $MnSe_x$ [15], VTe_2 [16], and VSe_2 [17, 18]. Ferromagnetism in $MnSe_x$ and VTe_2 was reported, yet the T_C was not determined experimentally [15, 16], and the origin of ferromagnetism in the 2D limit in $MnSe_x$ and VSe_2 is yet to be fully understood [19–26]. Especially, recent experimental examinations have evidenced a lack of intrinsic ferromagnetism in neither of VTe_2 nor VSe_2 [27–33]. During the preparation of this manuscript, we notice that bulk vdW Fe_5GeTe_2 has a T_C of about 310 K, while its few-layer samples have T_C of about 270 K, slightly lower than room temperature [34].

Cr_xTe_y has been one of the overlooked families in the hunt for room temperature vdW magnets. Among them, 1T-$CrTe_2$ is a layered compound with T_C of ~ 320 K in its bulk phase, making it a potential candidate for the investigation of 2D ferromagnetism [35]. In this work, we performed mechanical exfoliation of a bulk vdW crystal of 1T-$CrTe_2$, and found that the Curie temperature above 300 K for bulk $CrTe_2$ can be retained down to the few-layered limit. The ferromagnetism in few-layered $CrTe_2$ was further investigated in the framework of in-plane anisotropic magnetoresistance (AMR) at different temperatures. Our findings demonstrate that $CrTe_2$ might be a promising candidate for next generation room temperature spin-related 2D nanoelectronics.

2 Experimental

Bulk $CrTe_2$ was obtained by melting a molar mixture (Cr, K, Te) and further annealing for several days the mixture, from which K was eventually deintercalated (see Methods). The crystalline structure of the compound, with $P\bar{3}m1$ space group (Fig. 1(a)), was checked with powder X-ray diffraction (XRD), as shown in Fig. 1(b), with the measured diffraction peaks in good agreement with calculated ones as indicated below the green measured curve [36]. Inset of Fig. 1(b) shows the optical image of the as-grown bulk $CrTe_2$.

To further confirm the crystalline structure of the synthesized crystals, we used plane-view high-angle annular dark-field scanning transmission electron microscopy (HAADF-STEM) on an exfoliated $CrTe_2$ flake placed onto a lacey carbon grid (Fig. 1(c)). The Cr and Te atoms are arranged in an 1T symmetry, as indicated in schematic drawing (the same color code used as in Fig. 1(a), i.e., dark blue for Cr and light blue for Te) overlapped at the upper-right of the HAADF-STEM image. The measured distance between the nearest neighbor Te atoms from the HAADF-STEM is 2.4 Å, which is in agreement with the calculated value of 2.3 Å [36]. More experimental details on transmission electron mlcroscopy (TEM) characterization can be found in Fig. S1 in the Electronic Supplementary Material (ESM). Together with XRD and Raman spectra (discussed in the next paragraph), we can thus confirm the crystal structure of the material 1T-$CrTe_2$ studied in this work. Ultra-thin flakes of $CrTe_2$ are reported to show in-plane magnetism with Néel-like domain with lateral sizes of about 0.2–2 μm [37].

In order to study the magnetism of $CrTe_2$ in the 2D limit, we carried out mechanical exfoliation using the standard scotch tape method [38]. It is found that the yield of atomically thin $CrTe_2$ is rather low compared to those easily exfoliated layered compounds such as graphene, and the thinnest flake we could obtain was 3 nm (5 layers), as shown in the atomic force microscopy (AFM) topography in Figs. 1(d) and 1(e) (more AFM images can be found in Fig. S2 in the ESM). Moreover, similar to other telluride materials, few-layered $CrTe_2$ in air is

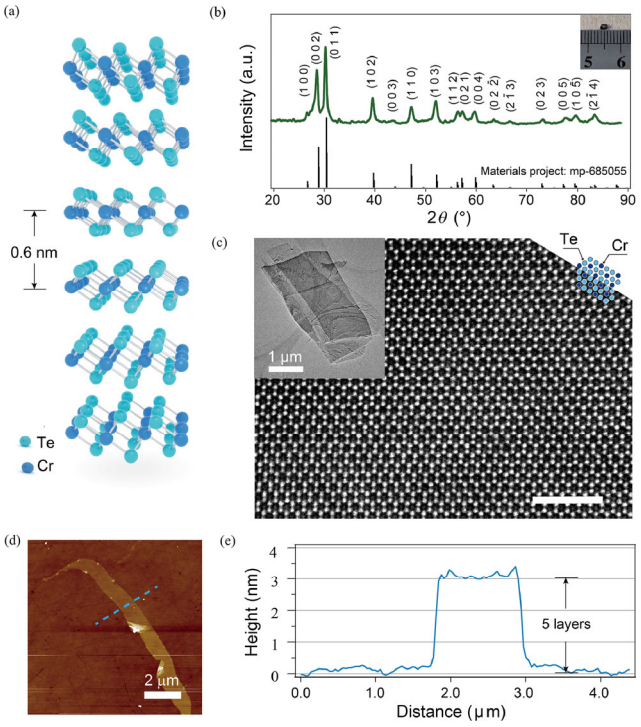

Figure 1 Structural characterizations of 1T-$CrTe_2$. (a) Schematics of the crystal structure of 1T-$CrTe_2$. (b) Powder XRD pattern of powdered bulk sample, with the calculated peaks in Ref. [36] plotted below. Inset of (b) shows the optical image of the as-grown bulk 1T-$CrTe_2$. (c) HAADF-STEM image of a 1T-$CrTe_2$ flake, whose low magnification TEM image is given in the inset. Scale bar is 2.5 nm. The schematic atoms (same color code as in (a)) in the up-right part in (c) indicate the arrangement of Cr and Te atoms as a top view of the vdW plane of 1T-$CrTe_2$. (d) AFM topographic image of a typical few-layered 1T-$CrTe_2$. (e) Height profile of the flake along the dashed line in (d).

easily degraded, preventing any further characterizations (Fig. S3 in the ESM). Therefore, protections such as hexagonal boron nitride (h-BN) encapsulation in a glove box, or Pt thin films capping layer in a vacuum evaporator, can be solutions to avoid air-degradation of ultra-thin $CrTe_2$ flakes. Indeed, Raman spectra of a 6 nm $CrTe_2$ (protected by encapsulating the $CrTe_2$ with two h-BN flakes in a glove box) measurements with a 633 nm laser, as given in Fig. 2(a), show that few-layered samples can be well preserved for a few days as its pristine ones (red circles), with two typical Raman peaks at about 100.0 and 134.1 cm^{-1}, while another 6 nm flake without any protection got rapidly degraded in air for several hours, with peaks shifted to 125.5 and 145.0 cm^{-1} (green circles). Raman spectroscopy thus supplies the fingerprints of pristine flakes, and thereby provides a quick and reliable way to select the non-degraded samples for further magnetic and electrical measurements (more details can be found in Figs. S4–S6 in the ESM).

3 Results and discussion

With protection of 5 nm Pt thin film, the thin layers of $CrTe_2$ were deposited onto transparent quartz substrates for Faraday measurements. Oblique incident probe beam with respect to the sample plane was applied to monitor the in-plane component of the magnetization in the few-layered $CrTe_2$ flakes (Fig. S7 in the ESM). Figure 2(b) shows characteristic ferromagnetic *M-H* loops at 10 K of $CrTe_2$ flakes with thickness of 8.7, 10, and 100 nm in green, yellow, and red, respectively. We also obtained Faraday rotation of a typical 10 nm h-BN encapsulated $CrTe_2$ flake at 300 and 320 K, respectively (Fig. S8 in the ESM), and

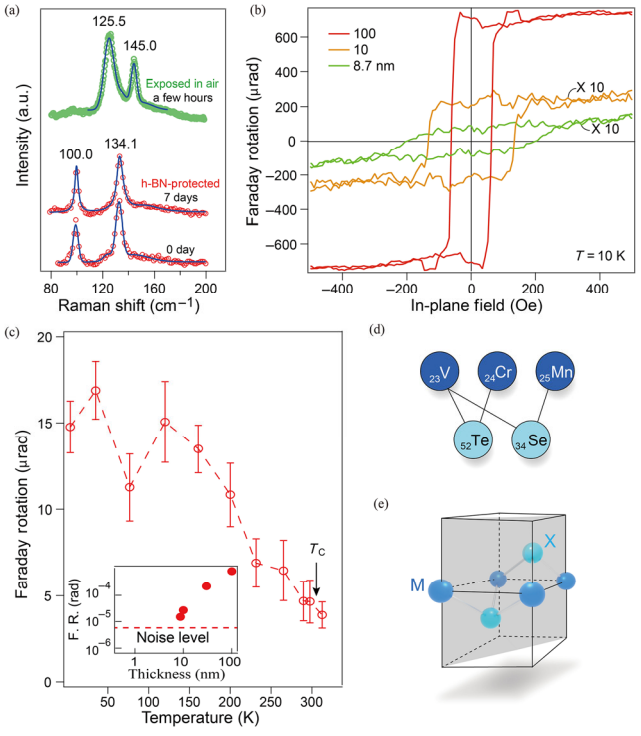

Figure 2 Magnetic properties of few-layered $CrTe_2$. (a) Raman spectra of a 6 nm $CrTe_2$ flake with (red circles) and without (green circles) air protection. Solid lines are fitted curves, with the fitted peak values indicated in the figure. (b) Faraday rotation of 5 nm Pt-thin film protected $CrTe_2$ flake with several thicknesses, data obtained at 10 K. For thin samples, signals are multiplied by a factor of 10 to fit the scale. (c) *M*–*T* curve extracted from the Faraday rotation at 400 Oe for the 8.7 nm $CrTe_2$ sample with Pt-thin film protection. T_C is found at around 305 K as indicated by the solid arrow. Inset shows the magnetic response with respect to sample thickness at 10 K. It is seen that as limited by the noise level of our setup, samples with thickness below 8 nm exhibit negligible signal. F. R. in the inset denotes Faraday rotation. (d) A summary of the four types of reported room temperature vdW ferromagnets. (e) Unit cell of MX_2.

it exhibits characteristic ferromagnetic *M*-*H* loops at 300 K, while the loop becomes a flat background above 320 K. It is noticed that the Faraday rotation signal decays significantly with decreasing sample thickness. For thin samples, signals are multiplied by a factor of 10 to fit the scale in Fig. 2(b). We extracted the saturated Faraday effect signal at B = 400 Oe, and thus obtained an effective *M*–*T* curve, for a 8.7 nm sample, shown in Fig. 2(c). The general trend in 8.7 nm $CrTe_2$ is rather similar to that measured in its bulk, with a T_C around 305 K in few-layered $CrTe_2$, as indicated by the solid arrow in Fig. 2(c).

Unlike the reported in bulk forms [35], no decomposing or phase transition was found in thin flake of $CrTe_2$, as it can reversibly undergo thermal cycles up to 350 K. We regret that because of the very weak Faraday rotation signal, the in-plane magnetism can be barely probed optically below 8 nm thickness. As shown in the inset of Fig. 2(c), we found that magnetic response at 10 K of samples about 8 nm in thickness reaches the limit of the noise level in our setup. Further improvement on optical measurement precision will be carried out in our future studies. It is known that magnetic interaction of few-layered vdW magnets may be vary from their bulk forms, depending on different systems [2, 18]. Here, the high T_C (still above room temperature, comparable to that of the bulk) in 8.7 nm $CrTe_2$ may speak of rather weak inter-layer magnetic interactions. It is also possible that surface degradation may happen, making the effective thickness thinner than the nominal thickness measured by AFM. An 8.7 nm sample may have a reduced actual thickness of the ferromagnetic part. Further examinations of the physical monolayer limit should be carried out in-situ in strictly all-vacuum conditions in our future studies.

Interestingly, for the transition metal dichalcogenide that are reported to be room temperature ferromagnets, VSe_2, $MnTe_2$, $MnSe_x$, and $CrTe_2$, all have a 1T phase, where the local coordination of the transition metal atoms and chalcogenide atoms form an octahedral (Figs. 2(d) and 2(e)). However, recent experiments have ruled out intrinsic ferromagnetism in epitaxial monolayer VTe_2 and VSe_2 [27–33]. Ultra-thin $CrTe_2$ seems to become the only known exfoliated ultra-thin vdW magnets with intrinsic long-range magnetic ordering above room temperature. The chalcogen atoms may play a key role in promoting ferromagnetism, because the close-to-90° angle of the metal-chalcogen-metal bonds is expected to promote a positive double super-exchange coupling. While the hybridization between the metal and chalcogen orbitals results in a strong contribution of metal orbitals to the density of states at the Fermi level (Fig. S9 in the ESM).

A mean-field solution to the Heisenberg model is employed [39, 40] to extract the Curie temperature $T_C = \frac{2zJS(S+1)}{3k_B}$, in which z is the coordination number (z = 6 in 1T MX_2), J is the exchange energy, and S is the spin angular momentum (orbital angular momentum L = 0 due to orbital quenching in octahedral MX_2). From the above equation, we extract J (Fig. S10 in the ESM). In our estimation, the mean-field treatment of pairwise interaction between spins is valid given that the product of spin fluctuations (deviation of spin away from its mean value) is small. Such a treatment is in principle independent on the dimensionality and can also be validated in 2D anisotropic magnets with strong magnetocrystalline anisotropy. Notice that magnetocrystalline anisotropy may affect the magnetic stability of 2D magnets, but does not contribute to the estimation of the exchange energy J [41, 42]. We also stress that several factors have been disregarded including the possible occurrence of charge density waves, as observed in VSe_2 and VTe_2 [17, 43]. A thorough understanding on the room temperature ferromagnetism in ultra-thin 1T-$CrTe_2$ remains an open question. We now come to the investigation of spin transport behaviour in few-layered $CrTe_2$. To protect the few-layered $CrTe_2$ we encapsulated it with different materials, including thin h-BN and Pt films (Fig. S11 in the ESM). In general, ultra thin $CrTe_2$ flakes were found to be stable as long as heating is avoided during the whole fabrication process. A typical h-BN-encapsulated device contacted with Au electrodes (see Methods) is shown in Figs. 3(a) and 3(b), for schematic and optical image, respectively. In our measurement, we notice that ultra-thin $CrTe_2$ samples exhibited no detectable anomalous Hall signals in transversal resistance R_{xy}. In the following, we mainly focus on the longitudinal resistance R_{xx}, with the configuration for measurements illustrated in Fig. 3(c).

Figure 3(d) shows R_{xx} at 2,250 Oe, recorded in a typical $CrTe_2$ device with a thickness of 10 nm, as a function of the angle θ between the in-plane magnetic field B and the electrical current J flowing between source and drain electrodes. A two-fold cos(2θ)-like oscillation is observed, similar to the case of more traditional ferromagnets [44, 45]. Figure 3(e) shows the corresponding magnetoresistance at 300 K for θ = 0°, and 90° in pink and blue lines, respectively (data taken at other temperatures are shown in Fig. S12 in the ESM). Unusual negative in-plane anisotropic magnetoresistance (AMR = $(R_{\parallel} - R_{\perp}) / R_{\perp}$) is observed in Fig. 3(e) and can be well reproduced in multiple samples as shown in Fig. S13 in the ESM.

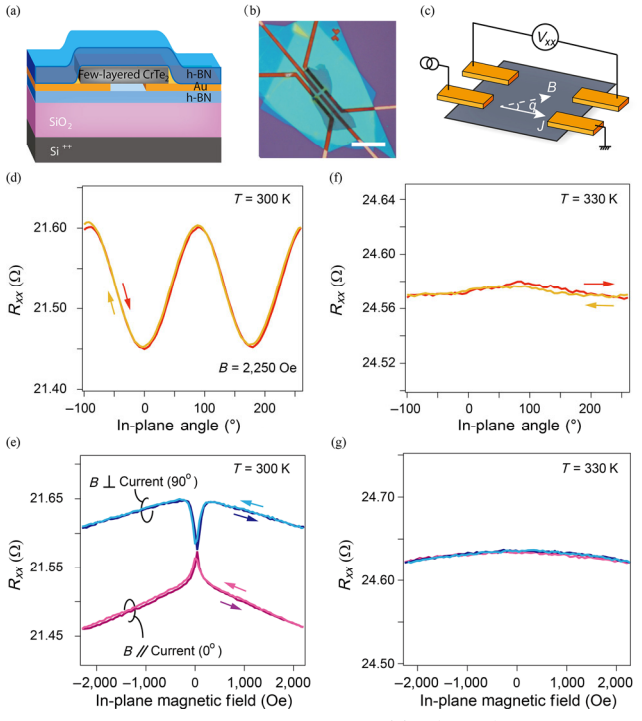

Figure 3 Anisotropic magnetoresistance of few-layered $CrTe_2$ at 300 K. (a) Art view and (b) optical image of a typical h-BN/$CrTe_2$/h-BN device. Scale bar in (b) is 10 μm. (c) Illustration of the measurement of in-plane magnetic field with an angle θ against the current J. (d) R_{xx} of 10 nm $CrTe_2$ as a function of θ with an 2,250 Oe magnetic field applied. (e) R_{xx} of few-layered $CrTe_2$ as a function of magnetic field B, with $\theta = 0°$ (pink lines) and 90° (blue lines), respectively. (f) and (g) are R_{xx} vs. θ, and R_{xx} vs. B with the same configurations as in (d) and (e) measured at 330 K.

It is noted that when heated up to 330 K, the AMR-related features disappear, and can be re-appear once the sample is cooled down to 300 K. This is a proof that the ferromagnetic-paramagnetic phase transition in few-layered $CrTe_2$ is reversible. Negative in-plane AMR (reproduced in multiple samples as shown in Fig. S13 in the ESM) is usually found in some conventional half-metallic ferromagnets such as Ni_3FeN [44], or Mn-doped Bi_2Se_3 [46]. In contrast, many band (itinerant) ferromagnets, such as Ni and Fe, [47] and especially vdW materials Fe_3GeTe_2 [48] (with much smaller AMR) have positive in-plane AMR. Here, the term half-metallicity (in magnetic systems such as Heusler alloys) refers to the case in which the majority-spin electronic states contribute overwhelmingly to electrical conduction at the Fermi level, whereas the minority-spin electrons have very low density of states (DOS) as if it were semiconducting. As will be discussed in the following part, in our case, the DOS of minority-spin is indeed much lower than that of the majority-spin electrons, which behaves half-metallicity-like.

Below 200 K, as shown in Fig. 4(a), the AMR deviates from the cos(2θ) behavior, and achieves an amplitude as high as 5% at 10 K, which is even comparable with the maximum values reported for NiFe alloys [49, 50]. Interestingly, the AMR changes its sign from negative into positive at low temperature. We show in Fig. 4(b) the R_{xx}–T curve for the same device (extracted from Fig. 4(a)) at $\theta = 0°$ (red solid line) and 90° (blue solid line), with a fixed in-plane magnetic field of 2,250 Oe. A crossing point can be seen in the boxed area (better visible in the zoom shown in the inset) at a temperature of about 26.5 K. More importantly, few-layer $CrTe_2$ shows a totally opposite AMR behaviour to some of these alloys, e.g., Ni_3FeN in the form of thin films, which have positive AMR at room temperature and negative AMR at low temperature [42].

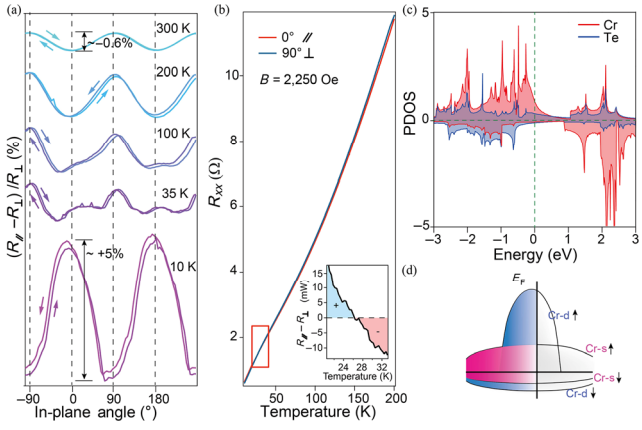

Figure 4 Mechanism of AMR in few-layered $CrTe_2$. (a) AMR ratio (r_{AMR}) of few-layered $CrTe_2$ at different temperatures. (b) R_{xx} as a function of temperature at $\theta = 0°$ (red line) and 90° (blue line). An in-plane magnetic field of 2,250 Oe was applied. Inset shows the difference between $R_{\parallel}$ and $R_{\perp}$, with negative and positive values separated at the temperature of about 26.5 K. (c) PDOS from both Cr and Te for spin up and spin down sub-bands calculated for monolayer $CrTe_2$. (d) Schematic image of the decomposed Cr s and d orbitals near the Fermi level.

To understand such a distinctive AMR in few-layer $CrTe_2$, we refer to the spin scattering model [51] in which the AMR ratio writes $r_{AMR} = \dfrac{R_{\parallel} - R_{\perp}}{R_{\perp}} \propto -(N_{\uparrow}^{d} - N_{\downarrow}^{d}) \cdot (\sigma_{\uparrow} - \sigma_{\downarrow})$ with $N_{\uparrow}^{d}$ and $N_{\downarrow}^{d}$ representing the electronic density of d states at E_F, of up and down spin, respectively. $\sigma_{\uparrow}$ and $\sigma_{\downarrow}$ are the electrical conductivity for up spin and down spin electrons, respectively. The competition between conducting electrons at each spin channel is the origin of the sign change of the AMR at different temperatures. From the calculated partial density of states (PDOS) of monolayer $CrTe_2$, as shown in Fig. 4(c) and Fig. S14 in the ESM, $N_{\uparrow}^{d}$ is much larger than $N_{\downarrow}^{d}$. Nevertheless, as illustrated in Fig. 4(d) (for more details refer to Fig. S14 in the ESM), at the Fermi level, the majority spin (↑) Cr d orbital is more localized than the minority spin (↓) Cr d orbital, meanwhile, Cr s orbitals for both spin polulation are delocalized. It is therefore expected that spin up electrons contribute to the minority of conductivity, due to a much larger magnitude of s-d scattering in the spin up channel than in the spin down channel, yielding $\sigma_{\uparrow} - \sigma_{\downarrow} < 0$, thus a positive AMR at low temperature. When thermal excitation takes over with increasing temperature, more spin up Cr d orbitals are occupied, suppressing s-d scattering and giving rise to a sign change in the $\sigma_{\uparrow} - \sigma_{\downarrow}$ term, thus a negative AMR up to 300 K.

4 Conclusions

In conclusion, we report room temperature ferromagnet in ultra-thin 1T-$CrTe_2$ vdW, which expands the magnetic vdW crystal toolbox. By magneto-optical and electrical measurements, ferromagnetism was demonstrated to be maintained in $CrTe_2$ below 8 nm, with a Curie temperature above 300 K and in-plane magnetic anisotropy. In addition to the unusual negative in-plane AMR at room temperature, the detailed spin transport measurement also found in the few-layered $CrTe_2$ the temperature-induced AMR sign change from −0.6 % AMR at 300 K to +5 % AMR at 10 K, which is opposite to that found in other itinerant vdW 2D ferromagnets, but can be understood based on the half-metallicity-like spin polarized band structure. Our studies reveal that the ultra-thin vdW ferromagnet $CrTe_2$ is a promising candidate for future room temperature spintronic

applications [52], since it can be, in principle, further implemented into in-plane spin-related nanoelectronics, such as microwave nano-oscillators [53] as well as large size flexible spin devices.

5 Methods

Synthesis. The $KCrTe_2$ compound has been prepared by mixing K, Cr, and Te under the Ar atmosphere of a glove box. This mixture was then placed in a sealed quartz tube and subsequently heated to melting temperature. It was maintained at 1,170 K for about 200 h. Next, the tube was opened, inside a glove box to avoid oxidation. De-intercalation of the alkali atoms (K) was performed via reaction with iodine (in excess) in acetronitrile, under constant stirring for about 2 h: $2KCrTe_2 + I_2 = 2CrTe_2 + 2KI$. The final product was rinsed in two steps, to eliminate the excess potassium iodide, first with acetonitrile, and then with acetone. The $CrTe_2$ crystals were eventually filtrated and dried under vacuum. The final products were shiny metal gray platelets with surface area up to 3 mm^2.

Material characterization. The TEM instrument is a Cs-corrected TEM (JEM-ARM300F) with an operation acceleration voltage of 200 kV. Powder XRD experiments were performed by the Bruker D8 ADVANCE diffractometer using the Cu Kα1 radiation (λ = 0.15406 nm) at room temperature, the voltage is 40 kV, and current is 40 mA. The h-BN (crystals from HQ Graphene) encapsulated $CrTe_2$ devices were fabricated using the dry-transfer methods [3] in a glove box. PDMS was used without any heating during the deposition of thin flakes. Spot size of about 2 μm diameter laser with wavelength of 800 nm was used. A Bruker Dimension Icon AFM was used for thicknesses and morphology characterizations. Samples shown in the ESM are measured in air shortly after the mechanical exfoliation of bulk crystal. An HR 800 JobinYvon Horiba polarized Raman spectrometer was used. Raman measurements were performed using a 633 nm laser, with nominal power of 1 mW. For the electrical measurements, a physical properties measurement system (PPMS, Quantum Design) and a probe station (Cascade Microtech Inc. EPS150) under ambient conditions were used.

Calculations. The electronic properties in this work were calculated by using the first-principles density functional theory as implemented in the Vienna *ab initio* simulation package (VASP) code [54]. The electron-ion interaction and electronic exchange-correlation interaction were respectively described by projector augmented wave (PAW) pseudopotentials [55] and the Perdew-Burke-Ernzerhof (PBE) [56] functional. The electronic kinetic energy cutoff for plane-wave basis was set to be 520 eV. The energy criterion for reaching self-consistency was set to be 10^{-8} eV. The Brillouin zones were sampled using the Γ-centered Monkhorst-Pack mesh by $20 \times 20 \times 1$ k-points and $40 \times 40 \times 1$ k-points for self-consistency and electronic density of states, respectively [57].

Acknowledgements

This work is supported by the National Key R&D Program of China (Nos. 2019YFA0307800, 2017YFA0206302, and 2017YFA0206200) and the National Natural Science Foundation of China (NSFC) (Nos. 11974357, U1932151, and 51627801). G. Q. Y. and X. F. H. thank the financial supports from the National Natural Science Foundation of China (NSFC) (No. 11874409). This work is supported by the National Natural Science Foundation of China (NSFC) (Nos. 61574060, and 8206300210). T. Y. acknowledges supports from the Major Program of Aerospace Advanced Manufacturing Technology Research Foundation NSFC and CASC, China (No. U1537204). Z. H. acknowledges the support from the Program of State Key Laboratory of Quantum Optics and Quantum Optics Devices (No. KF201816). The authors appreciate the help of Dr. Binbin Jiang in obtaining the HAADF-STEM images.

Electronic Supplementary Material: Supplementary material (including details of TEM images, EDS mapping, AFM scans, optical images, Raman spectra, schematic of the Faraday rotation measurement, Faraday rotation datas, DOS and PDOS datas, exchange energy and T_C diagram, fabrication methods and data, magnetoresistance data) is available in the online version of this article at https://doi.org/10.1007/s12274-020-3021-4.

References

[1] Huang, B.; Clark, G.; Navarro-Moratalla, E.; Klein, D. R.; Cheng, R.; Seyler, K. L.; Zhong, D.; Schmidgall, E.; McGuire, M. A.; Cobden, D. H. et al. Layer-dependent ferromagnetism in a van der Waals crystal down to the monolayer limit. *Nature* **2017**, *546*, 270–273.

[2] Gong, C.; Li, L.; Li, Z. L.; Ji, H. W.; Stern, Y., A.; Xia, Y.; Cao, T.; Bao, W.; Wang, C. Z.; Wang, Y. et al. Discovery of intrinsic ferromagnetism in two-dimensional van der Waals crystals. *Nature* **2017**, *546*, 265–269.

[3] Wang, Z.; Zhang, T. Y.; Ding, M.; Dong, B. J.; Li, Y. X.; Chen, M. L.; Li, X. X.; Huang, J. Q.; Wang, H. W.; Zhao, X. T. et al. Electric-field control of magnetism in a few-layered van der Waals ferromagnetic semiconductor. *Nat. Nanotechnol.* **2018**, *13*, 554–559.

[4] Jiang, S. W.; Shan, J.; Mak, K. F. Electric-field switching of two-dimensional van der Waals magnets. *Nat. Mater.* **2018**, *17*, 406–410.

[5] Deng, Y. J.; Yu, Y. J.; Song, Y. C.; Zhang, J. Z.; Wang, N. Z.; Sun, Z. Y.; Yi, Y. F.; Wu, Y. Z.; Wu, S. W.; Zhu, J. Y. et al. Gate-tunable room-temperature ferromagnetism in two-dimensional Fe_3GeTe_2. *Nature* **2018**, *563*, 94–99.

[6] Sun, Z. Y.; Yi, Y. F.; Song, T. C.; Clark, G.; Huang, B.; Shan, Y. W.; Wu, S.; Huang, D.; Gao, C. L.; Chen, Z. H. et al. Giant nonreciprocal second-harmonic generation from antiferromagnetic bilayer CrI_3. *Nature* **2019**, *572*, 497–501.

[7] Chen, W. J.; Sun, Z. Y.; Wang, Z. J.; Gu, L. H.; Xu, X. D.; Wu, S. W.; Gao, C. L. Direct observation of van der Waals stacking-dependent interlayer magnetism. *Science* **2019**, *366*, 983–987.

[8] Li, X. X.; Dong, B. J.; Sun, X. D.; Wang, H. W.; Yang, T.; Yu, G. Q.; Han, Z. Y. Perspectives on exfoliated two-dimensional spintronics. *J. Semicond.* **2019**, *40*, 081508.

[9] Song, T. C.; Cai, X. H.; Tu, M. W. Y.; Zhang, X. O.; Huang, B.; Wilson, N. P.; Seyler, K. L.; Zhu, L.; Taniguchi, T.; Watanabe, K. et al. Giant tunneling magnetoresistance in spin-filter van der Waals heterostructures. *Science* **2018**, *360*, 1214–1218.

[10] Wang, X.; Tang, J.; Xia, X. X.; He, C. L.; Zhang, J. W.; Liu, Y. Z.; Wan, C. H.; Fang, C.; Guo, C. Y.; Yang, W. L. et al. Current-driven magnetization switching in a van der Waals ferromagnet Fe_3GeTe_2. *Sci. Adv.* **2019**, *5*, eaaw8904.

[11] Li, Q.; Yang, M. M.; Gong, C.; Chopdekar, R. V.; N'Diaye, A. T.; Turner, J.; Chen, G.; Scholl, A.; Shafer, P.; Arenholz, E. et al. Patterning-induced ferromagnetism of Fe_3GeTe_2 van der Waals materials beyond room temperature. *Nano Lett.* **2018**, *18*, 5974–5980.

[12] Wang, C.; Zhou, X. Y.; Zhou, L. W.; Tong, N. H.; Lu, Z. Y.; Ji, W. A family of high-temperature ferromagnetic monolayers with locked spin-dichroism-mobility anisotropy: MnNX and CrCX (X = Cl, Br, I; C = S, Se, Te). *Sci. Bull.* **2019**, *64*, 293–300.

[13] Huang, C. X.; Feng, J. S.; Zhou, J.; Xiang, H. J.; Deng, K. M.; Kan, E. J. Ultra-high-temperature ferromagnetism in intrinsic tetrahedral semiconductors. *J. Am. Chem. Soc.* **2019**, *141*, 12413–12418.

[14] You, J. Y.; Zhang, Z.; Gu, B.; Su, G. Two-dimensional room-temperature ferromagnetic semiconductors with quantum anomalous Hall effect. *Phys. Rev. Appl.* **2019**, *12*, 024063.

[15] O'Hara, D. J.; Zhu, T. C.; Trout, A. H.; Ahmed, A. S.; Luo, Y. K.; Lee, C. H.; Brenner, M. R.; Rajan, S.; Gupta, J. A.; McComb, D. W. et al. Room temperature intrinsic ferromagnetism in epitaxial manganese

selenide films in the monolayer limit. *Nano Lett*. **2018**, *18*, 3125–3131.
[16] Li, J.; Zhao, B.; Chen, P.; Wu, R. X.; Li, B.; Xia, Q. L.; Guo, G. H.; Luo, J.; Zang, K. T.; Zhang, Z. W. et al. Synthesis of ultrathin metallic MTe_2 (M = V, Nb, Ta) single-crystalline nanoplates. *Adv. Mater*. **2018**, *30*, 1801043.
[17] Yu, W.; Li, J.; Herng, T. S.; Wang, Z. S.; Zhao, X. X.; Chi, X.; Fu, W.; Abdelwahab, I.; Zhou, J.; Dan, J. D. et al. Chemically exfoliated VSe_2 monolayers with room-temperature ferromagnetism. *Adv. Mater*. **2019**, *31*, 1903779.
[18] Bonilla, M.; Kolekar, S.; Ma, Y. J.; Diaz, H. C.; Kalappattil, V.; Das, R.; Eggers, T.; Gutierrez, H. R.; Phan, M. H.; Batzill, M. Strong room-temperature ferromagnetism in VSe_2 monolayers on van der Waals substrates. *Nat. Nanotechnol*. **2018**, *13*, 289–293.
[19] Onari, S.; Arai, T. Infrared lattice vibrations and dielectric dispersion in antiferromagnetic semiconductor $MnSe_2$. *J. Phys. Soc. Jpn*. **1979**, *46*, 184–188.
[20] Pollard, R. J.; McCann, V. H.; Ward, J. B. Magnetic structures of α-MnS and MnSe from ^{57}Fe Mossbauer spectroscopy. *J. Phys. C: Solid State Phys*. **1983**, *16*, 345–353.
[21] van Bruggen, C. F.; Haas, C. Magnetic susceptibility and electrical properties of VSe_2 single crystals. *Solid State Commun*. **1976**, *20*, 251–254.
[22] Bayard, M.; Sienko, M. J. Anomalous electrical and magnetic properties of vanadium diselenide. *J. Solid State Chem*. **1976**, *19*, 325–329.
[23] Liu, H. T.; Bao, L. H.; Zhou, Z.; Che, B. Y.; Zhang, R. Z.; Bian, C.; Ma, R. S.; Wu, L. M.; Yang, H. F.; Li, J. J. et al. Quasi-2D transport and weak antilocalization effect in few-layered VSe_2. *Nano Lett*. **2019**, *19*, 4551–4559.
[24] Jolie, W.; Knispel, T.; Ehlen, N.; Nikonov, K.; Busse, C.; Grüneis, A.; Michely, T. Charge density wave phase of VSe_2 revisited. *Phys. Rev. B* **2019**, *99*, 115417.
[25] Chen, P.; Pai, W. W.; Chan, Y. H.; Madhavan, V.; Chou, M. Y.; Mo, S. K.; Fedorov, A. V.; Chiang, T. C. Unique gap structure and symmetry of the charge density wave in single-layer VSe_2. *Phys. Rev. Lett*. **2018**, *121*, 196402.
[26] Feng, J. G.; Biswas, D.; Rajan, A.; Watson, M. D.; Mazzola, F.; Clark, O. J.; Underwood, K.; Marković, I.; McLaren, M.; Hunter, A. et al. Electronic structure and enhanced charge-density wave order of monolayer VSe_2. *Nano Lett*. **2018**, *18*, 4493–4499.
[27] Coelho, P. M.; Lasek, K.; Nguyen Cong, K.; Li, J. F.; Niu, W.; Liu, W. Q.; Oleynik, I. I.; Batzill, M. Monolayer modification of VTe_2 and its charge density wave. *J. Phys. Chem. Lett*. **2019**, *10*, 4987–4993.
[28] Wong, P. K. J.; Zhang, W.; Zhou, J.; Bussolotti, F.; Yin, X. M.; Zhang, L.; N'Diaye, A. T.; Morton, S. A.; Chen, W.; Goh, J. et al. Metallic 1T phase, $3d^1$ electronic configuration and charge density wave order in molecular beam epitaxy grown monolayer vanadium ditelluride. *ACS Nano* **2019**, *13*, 12894–12900.
[29] Wong, P. K. J.; Zhang, W.; Bussolotti, F.; Yin, X. M.; Herng, T. S.; Zhang, L.; Huang, Y. L.; Vinai, G.; Krishnamurthi, S.; Bukhvalov, D. W. et al. Evidence of spin frustration in a vanadium diselenide monolayer magnet. *Adv. Mater*. **2019**, *31*, 1901185.
[30] Coelho, P. M.; Nguyen Cong, K.; Bonilla, M.; Kolekar, S.; Phan, M. H.; Avila, J.; Asensio, M. C.; Oleynik, I. I.; Batzill, M. Charge density wave state suppresses ferromagnetic ordering in VSe_2 monolayers. *J. Phys. Chem. C* **2019**, *123*, 14089–14096.
[31] Duvjir, G.; Choi, B. K.; Jang, I.; Ulstrup, S.; Kang, S.; Thi Ly, T.; Kim, S.; Choi, Y. H.; Jozwiak, C.; Bostwick, A. et al. Emergence of a metal-insulator transition and high-temperature charge-density waves in VSe_2 at the monolayer limit. *Nano Lett*. **2018**, *18*, 5432–5438.
[32] Zhang, W.; Zhang, L.; Wong, P. K. J.; Yuan, J. R.; Vinai, G.; Torelli, P.; van der Laan, G.; Feng, Y. P.; Wee, A. T. S. Magnetic transition in monolayer VSe_2 via interface hybridization. *ACS Nano* **2019**, *13*, 8997–9004.
[33] Vinai, G.; Bigi, C.; Rajan, A.; Watson, M. D.; Lee, T. L.; Mazzola, F.; Modesti, S.; Barua, S.; Hatnean, M. C.; Balakrishnan, G. et al. Proximity-induced ferromagnetism and chemical reactivity in few-layer VSe_2 heterostructures. *Phys. Rev. B* **2020**, *101*, 035404.
[34] May, A. F.; Ovchinnikov, D.; Zheng, Q.; Hermann, R.; Calder, S.; Huang, B.; Fei, Z. Y.; Liu, Y. H.; Xu, X. D.; McGuire, M. A. Ferromagnetism near room temperature in the cleavable van der Waals crystal Fe_5GeTe_2. *ACS Nano* **2019**, *13*, 4436–4442.
[35] Freitas, D. C.; Weht, R.; Sulpice, A.; Remenyi, G.; Strobel, P.; Gay, F.; Marcus, J.; Núñez-Regueiro, M. Ferromagnetism in layered metastable 1T-$CrTe_2$. *J. Phys.: Condens. Matter* **2015**, *27*, 176002.
[36] Persson, K. Materials Data on $CrTe_2$ (SG: 164) by Materials Project. 2016[Online]. https://www.osti.gov/servlets/purl/1284084.
[37] Purbawati, A.; Coraux, J.; Vogel, J.; Hadj-Azzem, A.; Wu, N.; Bendiab, N.; Jegouso, D.; Renard, J.; Marty, L.; Bouchiat, V. et al. In-plane magnetic domains and Néel-like domain walls in thin flakes of the room temperature $CrTe_2$ van der Waals ferromagnet. *ACS Appl. Mater. Interfaces* **2020**, *12*, 30702–30710.
[38] Novoselov, K. S.; Geim, A. K.; Morozov, S. V.; Jiang, D.; Zhang, Y.; Dubonos, S. V.; Grigorieva, I. V.; Firsov, A. A. Electric field effect in atomically thin carbon films. *Science* **2004**, *306*, 666–669.
[39] Blundell, S. *Magnetism in Condensed Matter*; Oxford University Press: Oxford, 2001.
[40] Mohn, P. *Magnetism in the Solid State*; Springer-Verlag: Berlin, 2003.
[41] Mermin, N. D.; Wagner, H. Absence of ferromagnetism or antiferromagnetism in one-or two-dimensional isotropic Heisenberg models. *Phys. Rev. Lett*. **1966**, *17*, 1133–1136.
[42] Stanley, H. E.; Kaplan, T. A. Possibility of a phase transition for the two-dimensional Heisenberg model. *Phys. Rev. Lett*. **1966**, *17*, 913–915.
[43] Sugawara, K.; Nakata, Y.; Fujii, K.; Nakayama, K.; Souma, S.; Takahashi, T.; Sato, T. Monolayer VTe_2: Incommensurate Fermi surface nesting and suppression of charge density waves. *Phys. Rev. B* **2019**, *99*, 241404.
[44] Takata, F.; Kabara, K.; Ito, K.; Tsunoda, M.; Suemasu, T. Negative anisotropic magnetoresistance resulting from minority spin transport in $Ni_xFe_{4-x}N$ (x = 1 and 3) epitaxial films. *J. Appl. Phys*. **2017**, *121*, 023903.
[45] Tsunoda, M.; Komasaki, Y.; Kokado, S.; Isogami, S.; Chen, C. C.; Takahashi, M. Negative anisotropic magnetoresistance in Fe_4N film. *Appl. Phys. Exp*. **2009**, *2*, 083001.
[46] Zhang, D. M.; Richardella, A.; Rench, D. W.; Xu, S. Y.; Kandala, A.; Flanagan, T. C.; Beidenkopf, H.; Yeats, A. L.; Buckley, B. B.; Klimov, P. V. et al. Interplay between ferromagnetism, surface states, and quantum corrections in a magnetically doped topological insulator. *Phys. Rev. B* **2012**, *86*, 205127.
[47] McGuire, T.; Aboaf, J.; Klokholm, E. Negative anisotropic magnetoresistance in 3d metals and alloys containing iridium. *IEEE Trans. Mag*. **1984**, *20*, 972–974.
[48] You, Y. R.; Gong, Y. Y.; Li, H.; Li, Z. F.; Zhu, M. M.; Tang, J. X.; Liu, E. K.; Yao, Y.; Xu, G. Z.; Xu, F. et al. Angular dependence of the topological Hall effect in the uniaxial van der Waals ferromagnet Fe_3GeTe_2. *Phys. Rev. B* **2019**, *100*, 134441.
[49] Van Elst, H. C. The anisotropy in the magneto-resistance of some nickel alloys. *Physica* **1959**, *25*, 708–720.
[50] Bozorth, R. M. Magnetoresistance and domain theory of iron-nickel alloys. *Phys. Rev*. **1946**, *70*, 923–932.
[51] Kokado, S.; Tsunoda, M.; Harigaya, K.; Sakuma, A. Anisotropic magnetoresistance effects in Fe, Co, Ni, Fe_4N, and half-metallic ferromagnet: A systematic analysis. *J. Phys. Soc. Jpn*. **2012**, *81*, 024705.
[52] Hellman, F.; Hoffmann, A.; Tserkovnyak, Y.; Beach, G. S.; Fullerton, E. E.; Leighton, C.; MacDonald, A. H.; Ralph, D. C.; Arena, D. A.; Dürr, H. A. et al. Interface-induced phenomena in magnetism. *Rev. Mod. Phys*. **2017**, *89*, 025006.
[53] Awad, A. A.; Dürrenfeld, P.; Houshang, A.; Dvornik, M.; Iacocca, E.; Dumas, R. K.; Åkerman, J. Long-range mutual synchronization of spin Hall nano-oscillators. *Nat. Phys*. **2017**, *13*, 292–299.
[54] Kresse, G.; Furthmüller, J. Efficient iterative schemes for *ab initio* total-energy calculations using a plane-wave basis set. *Phys. Rev. B* **1996**, *54*, 11169–11186.
[55] Kresse, G.; Joubert, D. From ultrasoft pseudopotentials to the projector augmented-wave method. *Phys. Rev. B* **1999**, *59*, 1758–1775.
[56] Perdew, J. P.; Burke, K.; Ernzerhof, M. Generalized gradient approximation made simple. *Phys. Rev. Lett*. **1996**, *77*, 3865–3868.
[57] Monkhorst, H. J.; Pack, J. D. Special points for Brillouin-zone integrations. *Phys. Rev. B* **1976**, *13*, 5188–5192.